

Green synthesis of α - Fe_2O_3 nanoparticles for arsenic(V) remediation with a novel aspect for sludge management



Debarati Mukherjee^{a,b}, Sourja Ghosh^{a,b,*}, Swachchha Majumdar^b, K. Annapurna^{a,c}

^aAcademy of Scientific and Innovative Research (AcSIR), CSIR–Central Glass and Ceramic Research Institute, India

^bCeramic Membrane Division, CSIR–Central Glass and Ceramic Research Institute, 196, Raja S.C. Mullick Road, Kolkata 700032, India

^cGlass Science and Technology Section, Glass Division, CSIR–Central Glass and Ceramic Research Institute, 196, Raja S.C. Mullick Road, Kolkata 700032, India

ARTICLE INFO

Article history:

Received 30 September 2015

Received in revised form 28 November 2015

Accepted 8 December 2015

Available online 11 December 2015

Keywords:

Aloe vera

Iron oxide nanoparticle

Arsenic removal

Response surface methodology

Sludge management

ABSTRACT

A simple, single step and eco-friendly approach was taken for synthesizing iron oxide nanoparticles using *Aloe vera* leaf extract. The nanoparticles were characterized by various techniques and used for arsenic(V) remediation in synthetic system with an initial concentration range of 2–30 mg/L. The effect of pH, particle dosage and initial arsenic concentration on arsenic adsorption was investigated using response surface methodology involving five levels Central Composite Design (CCD) considering adsorption capacity as the response. The nanoparticles showed a high sorption capacity of 38.48 mg/g in the experimental range of concentration compared to other inorganic oxide based adsorbents.

A novel approach was adopted for utilization of arsenic contained sludge. As(V) sorbed nanoparticles were used in the preparation of colored soda lime silicate glass. The basic properties such as density, thermal and optical properties were measured for the experimental glass sample and compared with samples containing commercial Fe_2O_3 .

The overall study indicates that the green synthesized iron oxide nanoparticle is a prospective candidate for arsenic remediation in contaminated water. The arsenic contained sludge may be used in preparation of coloured glasses which have wide application in making container bottles and building glasses.

© 2015 Elsevier Ltd. All rights reserved.

1. Introduction

Nanotechnology has introduced a new dimension in the field of environmental remediation of various toxic contaminants like heavy metals, dyes and pesticides etc. Controlling the particle size and shape at nanoscale results into a large surface area to volume ratio which imparts greater reactivity. Apart from the smaller particle sizes, presence of a large numbers of active sites and the catalytic potential of nanoparticles enable them as potential candidates for wide range of contaminants [1]. Nanoscale iron particles have shown efficiency for detoxification of chlorinated organic solvents, organochlorine pesticides and PCBs [2]. Zhang et al. prepared ferromagnetic carbon coated Fe nanoparticle which could remove over 95% of chromium (VI) in wastewater [3]. Manganese based nanoparticle synthesized using micro-emulsion process and coated with gold was observed as efficient nano-sorbents for removal of heavy metals from wastewater [4]. Copper

(II) oxide nanoparticles synthesized by thermal refluxing process were found as a potential nano-adsorbent for arsenic removal [5].

Iron oxide based components have a natural affinity for arsenic sorption [6]. Removal of As(V) using magnetic Fe_3O_4 from municipal waste water has been reported [7]. Fe(III) crosslinked alginate nanoparticles were used in fixed bed column for arsenic (V) removal [8]. Apart from being an effective adsorbent of As(V), the nano-sorbent demonstrated antimicrobial property also. The adsorption–desorption behaviour for As(V) was studied using hydrated iron oxide particles in combination with a macroporous ion-exchange resin at neutral pH [9]. A novel composite material was developed with high arsenic adsorption capacity by encapsulating γ - Fe_2O_3 nanoparticles in macroporous silica [10].

Most of the research studies focus on synthesis of iron oxide nanoparticles by chemical route using reducing agents [11]. Chemical reagents are often toxic, flammable and expensive in nature. In the process of synthesizing magnetite nanoparticles using toxic solvents, hazardous byproducts may generate and the process involves high energy consumption [12]. Therefore, biogenic or green synthesis of nanoparticles has emerged as an environment friendly and promising approach. Application of

* Corresponding author at: CSIR–Central Glass and Ceramic Research Institute, 196, Raja S.C. Mullick Road, Kolkata. Fax: +91 33 2473 0957.

E-mail addresses: sourja@cgcrici.res.in, sourja.g@gmail.com (S. Ghosh).

various plant extracts has been reported for biosynthesis of gold and silver nanoparticles using rapid and nontoxic process [13]. Presence of different phytochemicals, viz. glutathiones, polyphenols, alkaloids as well as various types of proteins, enzymes, polysaccharides and alcoholic compounds in plant extracts facilitate reduction of metal ions and formation of stable nanoparticles [12]. Extracts of *Aloe vera* leaves were used for production of silver nanoparticles and its antimicrobial activity has been studied [14]. The gel of *A. vera* leaf acts as a bio-reducing agent for preparation of metal oxide and metal nanoparticle, semiconductors, etc. [15]. Nanocrystalline zinc-aluminate had been synthesized using *A. vera* leaf extract [15]. Biosynthesis of iron oxide nanoparticles with less than 5 nm were achieved in preferential cubic arrays deriving into magnetite and wuestite-like clusters using alfalfa [16].

The present study is oriented towards developing an effective and eco-friendly solution using iron oxide nanoparticles for arsenic remediation in highly arsenic contaminated water. Although various morphologies of haematite crystals had been developed earlier [17–19], however the necessity for developing a simple and appropriate method for synthesis of controlled sized hematite crystals still exists [11]. In the current study haematite (α -Fe₂O₃) nanoparticles have been synthesized using a simple and single step green procedure using *A. vera* plant extract. Leaf extracts of *A. vera*, a traditional medicinal plant containing various phytochemicals like flavonoids, tannin, saponin, sterols along with organic acids, polysaccharides and different enzymes [20]. Although the plant extract had been used in synthesis of gold and silver nanoparticles [21,22], phytochemical synthesis of α -Fe₂O₃ nanoparticles using *A. vera* extract has not been reported till date. In the present study green synthesis of α -Fe₂O₃ nanoparticles (FeIII-NP) has been attempted using *A. vera* leaf extract and the potential of the synthesized nanoparticles has been explored for arsenic(V) remediation in synthetic aqueous system. This method of synthesis employs cost-effective, environment friendly, non-toxic precursors and is a simple and time saving process [15] unlike the conventional chemical routes. Response surface methodology (RSM) was employed using the As(V) adsorption capacity of developed nanoparticles as the response to optimize different parameters involved in arsenic adsorption, viz. solution pH, nanoparticle dosage and initial arsenic concentration. The statistical analysis based on Central Composite Design (CCD) was undertaken to evaluate the overall interactive influences on the experimental response and to identify the relationship between the response and the independent variables in an efficient manner compared to the conventional processes.

Sludge management in arsenic remediation technologies is a major issue which needs special attention from the environmental perspectives. As the arsenic rich sludge cannot be disposed to landfill, the objective is to reuse the sludge for beneficial purpose. Application of ingredients like lime, cement, clay, etc. had been reported for solidification of the sludge in producing construction materials like bricks [23]. A novel application had been explored for arsenic sludge management in the present study. As(V) containing α -Fe₂O₃ nanoparticle sludge was utilized in the preparation of coloured soda lime silicate glass. Generally iron is avoided in common glass making. However for special/functional glasses like amber glasses, heat absorbing glasses and container glasses, iron needs to be incorporated. This motivated us to use the arsenic contaminated iron oxide sludge in glass making. Presence of As(V) acts as a refining agent [24] and helps in the reduction of bubbles during melting, thus facilitates homogenization of the glass sample. The basic properties such as density, thermal and optical properties of the glass sample were measured along with examination of bubbliness and compared with that of soda lime silicate glass prepared with doping of commercial Fe₂O₃. The

produced glass may have a wide application in container bottles and also as building glasses.

2. Materials and methods

2.1. Synthesis of nanoparticles

Anhydrous ferric chloride (FeCl₃) of AR grade obtained from Merck, Germany was used as the initial precursor. *A. vera* leaves were collected from nearby garden and washed thoroughly with distilled water to eliminate dust and other surface impurities. The leaves were cut into small pieces, ground and boiled with small amount of distilled water for 10 min to obtain a thick, viscous gel which was subsequently filtered and stored at cold condition. 10 g anhydrous FeCl₃ was added to 100 cc of this extract with 1:10 w/v ratio and kept under heating and stirring mode at 250 °C and 300 rpm respectively. Heating was conducted in a closed conical flask. Change of colour from yellow to brownish black was observed within about 10 min indicating formation of iron oxide nanoparticles. The solution was evaporated to dryness to separate the formed nanoparticles. The particles were washed with distilled water for several times and centrifuged to separate the supernatant. The material obtained was dried in air oven and kept in air tight container for further use.

2.2. Characterization of nanoparticles

The synthesised nanoparticles were characterized by X-ray Diffraction technique to predict the crystallinity as well as the phase of the compound. The XRD analysis was performed using Philips 1710 diffractometer with starting position $2\theta = 20.02^\circ$ to end position $2\theta = 79.97^\circ$ having step size $2\theta = 0.05^\circ$ using Cu as anode material ($\alpha = 1.541 \text{ \AA}$) at 25 °C. The morphology and microstructure of the powder material was studied using field emission scanning electron microscopy (FESEM, Zeiss, Germany). In addition, the qualitative energy dispersive spectroscopy (EDS) spectra analysis was undertaken to know the elemental composition of the particles. The morphology of the powder was further confirmed by Transmission Electron Microscopy (TEM) analysis (Technai G2, 30ST (FEI, USA) instrument). The oxidation states of iron and oxygen in the synthesized nanoparticle was analyzed by X-ray photoelectron spectroscopy technique using PHI 5000 XPS-analyzer, (Versaprobe-II, USA). The particle size of the synthesized powder was measured using particle size analyzer (Zetasizer, Nanoseries, Malvern). Specific surface area of nanoparticle was determined by adsorption-desorption of nitrogen using multi-point Braunauer-Emmett-Teller (BET) method using Quantachrome Autosorb Automated Gas Sorption System, (USA). Fourier transform infrared spectroscopy (FTIR, PerkinElmer, USA) was employed for identification of various functional groups in the synthesized FeIII-NP within the range of 400 cm⁻¹–4500 cm⁻¹. The arsenic adsorbed nanoparticle sample was characterized in terms of FTIR and FESEM analysis to identify any possible changes in FeIII-NP after arsenic sorption.

2.3. Batch mode study with arsenic(V) and optimization of process parameters by response surface methodology

Standard As(V) solution of 1000 mg/L obtained from Merck, Germany was used as the stock solution for adsorption experiments. As(V) solution of a certain initial concentration was taken in 50 mL conical flasks, pH was adjusted and FeIII-NP was incorporated at a certain dosage. The solutions were stirred at 150 rpm for 12 h in controlled temperature, filtered using 0.2 μm PVDF disposable syringe filters and analysed for As(V) concentration

using UV–vis spectrophotometer [ZEN 2600] of Varian, Australia [25].

Adsorption experiments were performed according to an experimental design set up using Central Composite Design (CCD). The influencing parameters like solution pH, adsorbent dosage and initial As(V) concentration were then optimised by response surface methodology. RSM consists of statistical methods which are used to derive a relationship between the experimental response and associated controllable input variables and subsequently to find out the significance of these variables. The most popular is the Central Composite Design (CCD) which is used for fitting quadratic models [26,27]. The number of experimental runs (N) in CCD with n number of variables is represented as below [28]:

$$N = 2^n + 2n + n_c \quad (1)$$

where 2^n is the number of factorial run, $2n$ is the number of axial runs and n_c is the centre runs. In CCD, all the influencing factors are studied in five levels, namely $-\alpha$, -1 , 0 , $+1$, $+\alpha$. The value of α [28] is calculated as below:

$$\alpha = 2^{(n-n_c)/4} \quad (2)$$

For statistical calculations, variables X_i are coded as below according to [29]:

$$X = (X_i - X_0)/\Delta X \quad (3)$$

where X_i is the dimensionless coded value of i th independent variable, X_0 is the value of X_i at the centre point, ΔX is the step change value. In the present study, equilibrium parameters influencing the adsorption capacity for As(V) were studied. The adsorption capacity q_e is estimated as below:

$$q_e = V(C_0 - C_e)/m \quad (4)$$

where C_0 is the initial As(V) concentration, C_e is the equilibrium As(V) concentration, V is the volume of As(V) solution and m is the mass of the adsorbent. In this study pH, initial As(V) concentration and adsorbent dosage were selected as independent input variables and adsorption capacity as the dependent experimental response. The experimental range and levels of the independent process variables are shown in Table 1. Experimental design having 6 replicates at centre point, 6 experiments at axial points with a total of 20 experiments was set up. The α value was chosen to be face-centered ($\alpha = 1$) indicating that the axial points are placed on the cube portion of the design. This is adopted when cube points of the design are the operational limits [30]. The design of the experimental runs as set up by CCD is represented in Table 2.

2.4. Utilization of arsenic rich sludge in glass preparation

The composition selected for formation of two batches, each 100 g of colored soda-lime silicate glass involved SiO₂ 74%, Al₂O₃ 1.3%, Na₂O 12.3%, K₂O 1.5%, CaO 10.5%, Fe₂O₃ 0.3% and TiO₂ 0.1%, respectively. The raw materials used were fine chemicals from Sigma Aldrich. The starting chemicals comprise SiO₂, Al₂O₃, Na₂CO₃, K₂CO₃, CaCO₃, Fe₂O₃ and TiO₂ of purity 99.9%. A Set of two glasses was prepared considering arsenic adsorbed iron oxide

nanoparticle as raw material in one (experimental batch) while in the other commercial Fe₂O₃ was employed (control batch). Arsenic content was 1.216 mg in the experimental batch with 0.3 g Fe₂O₃.

The soda lime silicate glasses were prepared by rapid melting–quenching technique. The appropriate quantities of chemicals for yielding each batch of 100 g glass were accurately weighed and mixed using a mortar and pestle to impart homogeneity to the glass batch. The mixture was placed in a platinum crucible which was kept in the furnace at 1450 °C. The temperature was increased to 1550 °C at which melting of the batch occurs. The temperature was maintained for 1.5 h accompanied by two intermittent stirrings with an interval of 30 min. The melt was then taken out and cast in a mould to give the desired shape. The cast glass block was immediately transferred to an annealing furnace where it was annealed at 650 °C for 2 h followed by slow cooling to room temperature to release the internal stress.

Both the glass blocks were characterized to observe their physical appearance, density and transmission spectra. The glass blocks were observed under an optical microscope [Leica M165C, USA], to see the presence of bubbles. Thermogravimetric and differential thermal analysis (TGA/DTA) was conducted using a Thermogravimetric Analyzer [NETZSCH, Germany]. Density was measured following Archimedes principle on a digital balance [Mettler Toledo] equipped with density kit using double distilled water as buoyancy liquid. The transmittance of the polished glass samples was measured using a UV–vis–NIR spectrophotometer [Shimadzu 3100] in the range 200 nm to 2500 nm.

3. Results and discussions

3.1. Synthesis and characterizations of iron oxide nanoparticles

Iron oxide nanoparticle was synthesised from anhydrous ferric chloride precursor by green route using *A. vera* extract. The formation of nanoparticles was confirmed by various characterization techniques, viz. XRD, FESEM, TEM and XPS.

The X-ray diffraction pattern is shown in Fig. 1. The peaks at 2θ value of 26.868°, 32.679°, 35.41°, 39.23°, 56.04° and 67.99° corresponds to α -Fe₂O₃ having a hexagonal phase (space grouping R3c (167) with JCPDS file no.-33-0664). The broader peaks indicate the particles to be of very small size in the nanometre range [15]. The crystallite size was estimated from the width of (110) plane according to the Scherrer's formula $D = k\lambda/\beta \cos\theta$, where constant k is 0.9–1, β is the full width half maxima and θ is the Bragg angle. The size was found to be 5.5 nm.

The morphology of the powders observed from the FESEM images indicate rod shaped particles which are in an agglomerated state (Fig. 2a). In green synthesis of nanoparticles, capping agents play an important role in controlling the shape and size of nanoparticles. They bind nonspecifically to different sites causing anisotropic growth in any direction [31]. In our study also, the capping agents in *A. vera* extract like amino acids may control the shape of nanoparticles, causing anisotropic growth in a certain direction resulting in rod shaped nanoparticles. The qualitative energy dispersive X-ray spectroscopy (EDX) spectra showed the presence of Fe and O at different positions due to emission from different orbitals. The particle size from SEM is estimated to be about 100 nm.

The TEM analysis in Fig. 2(b) indicates bright field imaging mode showing rod shaped particles with dimensions of 100 nm \times 20 nm (length \times width) which is in well agreement with the earlier observations. Selected area diffraction pattern (SAED) shows ring patterns surrounded by particles which reveal the polycrystalline nature of the synthesized powders. The d_{spacing}

Table 1
Experimental range and levels of independent input variables.

Independent variable	Range and Level		
	−1	0	+1
pH (A)	6	7	8
Adsorbent dose (g/L) (B)	0.5	1.25	2
Initial As(As(V)) concentration (mg/L) (C)	2	16	30

Table 2
Actual and predicted values.

Runs	Uncoded values			Sqrt adsorption capacity (mg/g) (Y)	
	Factor A: pH	Factor B: dosage(g/L)	Factor C: concentration (mg/L)	Experimental response	Predicted response
1	7.00	1.25	16.00	3.83	3.62
2	8.00	2.00	2.00	1.13	1.18
3	6.00	2.00	30.00	3.97	3.84
4	7.00	1.25	16.00	3.46	3.62
5	6.00	0.50	2.00	2.33	2.47
6	8.00	0.50	30.00	8.01	7.97
7	7.00	1.25	16.00	3.77	3.84
8	6.00	2.00	2.00	1.15	1.22
9	7.00	1.25	16.00	3.8	3.74
10	8.00	2.00	30.00	4.1	4.0
11	8.00	0.50	2.00	2.3	2.47
12	6.00	0.50	30.00	8.15	8.14
13	7.00	1.25	16.00	3.68	3.70
14	7.00	1.25	16.00	3.28	3.70
15	7.00	1.25	2.00	1.46	1.04
16	7.00	1.25	30.00	4.89	5.17
17	7.00	0.50	16.00	6.05	5.8
18	8.00	1.25	16.00	4.89	5.17
19	7.00	2.00	16.00	3.02	3.13
20	6.00	1.25	16.00	3.82	3.76

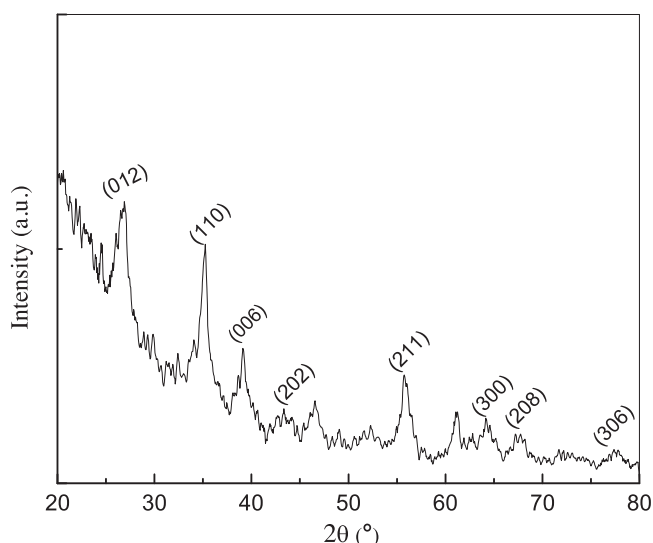


Fig. 1. XRD analysis of FeIII-NP sample.

values match with those obtained from XRD data showing presence of (110) and (202) planes.

The full XPS surface spectra of FeIII-NP sample confirm the presence of Fe and O elements in the nanoparticle sample (Fig. 3). The core level spectra of Fe shows peaks at 710.24 eV and 723.34 eV which corresponds to binding energies of Fe 2p_{3/2} and Fe 2p_{1/2}, respectively with doublet separation (ΔE) of 13.10 eV. These peak positions are in well agreement with Fe⁺³ of α -Fe₂O₃ [32]. The deconvoluted core level spectra of O1s shows two peaks, one at 528.5 eV which matches with standard datasheet values corresponding to the Fe—O bond in Fe₂O₃ [33] and the other at 530.9 eV which corresponds to C=O bond of aromatic compounds [34]. This is due to the unreacted organic components present in *A. vera* leaf extract which are retained in nanoparticles.

The FTIR spectra of the FeIII-NP sample are represented in Fig. 4 showing peaks at 665 cm⁻¹ and 460 cm⁻¹ which can be assigned to the Fe—O—Fe stretching vibrations [35]. The band at 3384 cm⁻¹ is assigned to O—H stretching vibration and 1629 cm⁻¹ due to C=O

stretching vibrations [35] due to the presence of unreacted ketone groups of the organic compounds like chromones and flavones present in leaf extract [36] while that corresponding to 858 cm⁻¹ may be due to α -glycosides [37].

The average particle size of the synthesized powder was found to be 99.5 nm (Zetasizer, Nanoseries). The measurement is based on the process of dynamic light scattering (DLS) method wherein the Brownian motion of the particles is measured and related to the particle size. The particles are illuminated and intensity fluctuations in the scattered light are measured. The intensity versus diameter plot depicted an almost unimodal distribution with d_{50} of 99.5 nm (figure not shown). Specific surface area of α -Fe₂O₃ was determined by adsorption–desorption of nitrogen on Quantachrome Autosorb Automated Gas Sorption System, (Boynton Beach, FL, USA) using multipoint Braunauer–Emmett–Teller (BET) method. The surface area was found to be 18.8 m²/g. The average pore diameter, pore volume and pore size distributions were found from nitrogen adsorption–desorption isotherms using Barret–Joyner–Halender (BJH) method. Average pore diameter of 275.1 Å and pore volume of 0.0378 cc/g are much higher and these are an important characteristic for better adsorption.

Leaf extract of *A. vera* is a heterogeneous mixture with 98.5% water while the rest portion comprises of a large range of compounds including components like anthraquinones, carbohydrates and saccharides, vitamins, enzymes, chromones, amino acids and proteins, etc. [38]. The concentration of the organic components as calculated on dry matter basis involves 73.35% crude fibre which comes from the carbohydrate and polysaccharides, 6.81% crude protein and 2.91% crude fat [39]. The organic polysaccharides and anthraquinones may contribute in the formation of iron oxide nanoparticles while the amino acids may act as capping agents for the formed nanoparticles. The pH of the *A. vera* extract was found to be 8.2 indicating its alkaline nature which helped in conversion of anhydrous FeCl₃ to ferric hydroxide Fe(OH)₃. The Fe(OH)₃ may be subsequently converted to α -Fe₂O₃ in presence of biomolecules like the polysaccharides present in the *A. vera* extract. The formed nanoparticles may be stabilised by amino acids like alanine, glycine, etc. by formation of chelating compounds [40]. These amino acids have amino group at one end and carboxylate group at other end both of which can take part in complexation with the metal ion. Iron(III) being a transition element forms complex with the amino group [40] which helps to

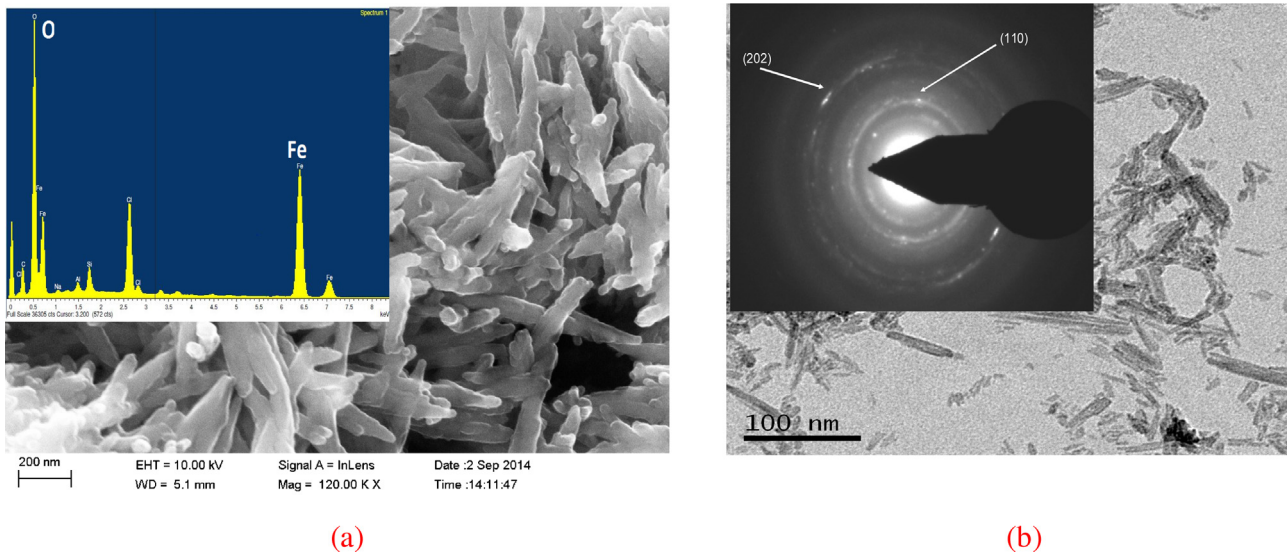


Fig. 2. Microscopic image of the synthesized FeIII-NP sample as such, (a) FESEM with EDX analysis (inset); (b) TEM image with SAED pattern (inset). (For interpretation of the references to color in the text, the reader is referred to the web version of this article.)

prevent further nucleation and hence aggregation of the nanoparticles. The presence of unreacted components in *A. vera* leaf extract may be observed from the FTIR spectra where peaks at 1629 cm^{-1} and 858 cm^{-1} are due to the organic constituents [40].

3.2. Arsenic(V) adsorption using Fe-NP: statistical analysis using RSM

Experiments involving batch mode adsorption study with arsenic(V) were performed according to experimental design set up using CCD and the corresponding experimental and predicted response values are represented in Table 2. The experimental As(V) concentrations as prepared were 34.014, 18.78 and 2.87 mg/L respectively for design prediction of 30, 16 and 2 mg/L, respectively. Accordingly, a regression model equation was developed for arsenic adsorption. Usually a quadratic model is used in RSM to

find a relationship between the independent variables and the dependent response which is represented as:

$$y = \beta_0 + \sum \beta_i x_i + \sum \beta_{ii} x_i^2 + \sum \beta_{ij} x_i x_j \quad (5)$$

where y is the response, x_i and x_j are independent process variables, while $\beta_0, \beta_i, \beta_{ii}$ and β_{ij} represent the regression coefficients for intercept, linear, quadratic and interaction terms, respectively.

In the present study, second order quadratic model is used to describe relationship among the controllable input parameters, viz. pH (A), FeIII-NP dose, g/L (B), initial As(V) concentration, mg/L (C) and the response, i.e. the adsorption capacity, mg/g (Y). Since ratio of maximum to minimum response is >10 , square root transformation is employed. The empirical model in terms of

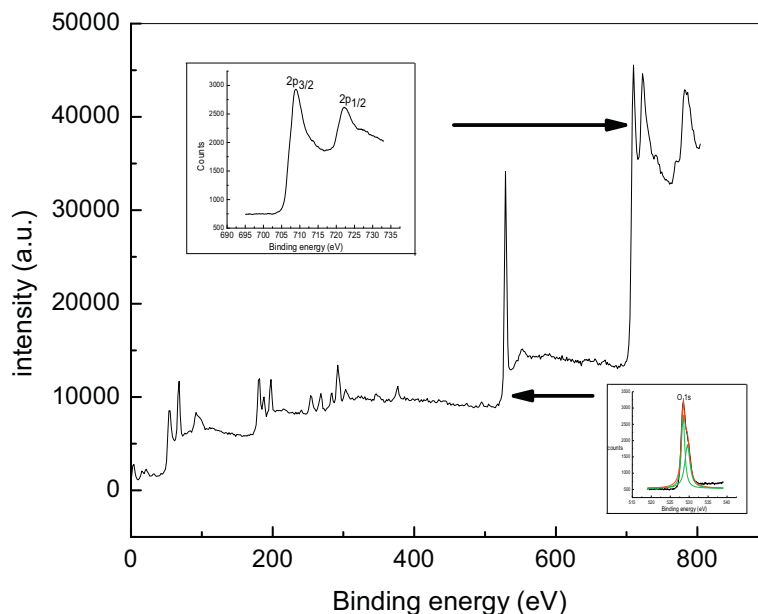


Fig. 3. Surface and core level XPS analysis of the synthesized FeIII-NP sample.

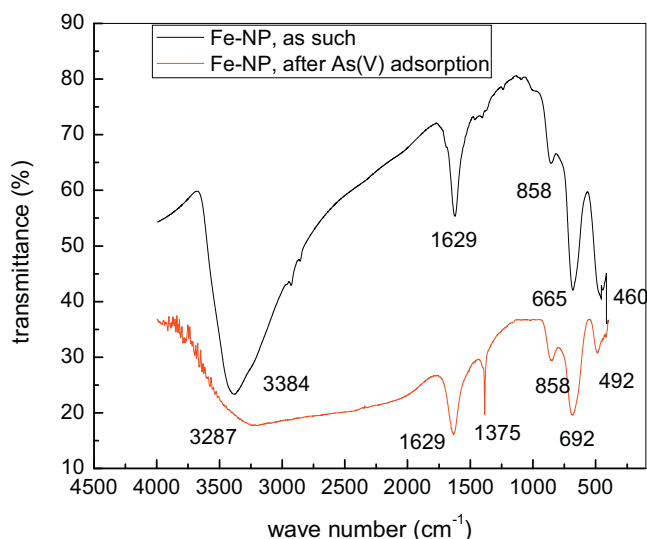


Fig. 4. FTIR analysis of FeIII-NP as such and after arsenic(V) adsorption.

coded factors is obtained as:

$$\begin{aligned} \text{Sqrt Adsorption Capacity}(Y) = & +3.68 - 0.022 \times A - 1.33 \times B \\ & + 2.06 \times C + 0.041 \times A^2 + 0.77 \\ & \times B^2 - 0.59 \times C^2 + 0.052 \times A \times B \\ & - 0.011 \times A \times C - 0.70 \times B \times C \quad (6) \end{aligned}$$

3.3. Analysis of variance (ANOVA) for response surface quadratic model

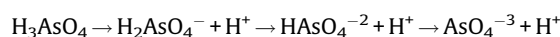
The ANOVA result for the adsorption of arsenic has been presented in Table 3. To develop a statistically significant regression model, the insignificant terms ($p > 0.05$) have been eliminated. The results indicate that B , C , BC , B^2 and C^2 are significant terms ($p < 0.05$) while A has no such effect on the adsorption capacity. Eq. (5) is used to find the effects of the parameters on the response. The experimental and predicted values are shown in Table 3. The model F value of 81.55 implies the model is significant.

A good fit between the experimental and predicted response is clarified from the value of the coefficient of determination (R^2) of the model. R^2 value was 0.9828 which implies that 98.28% of the

variations for As(V) adsorption capacity are explained by the independent variables while only 1.72% of variations cannot be explained by the model. The difference between the predicted R^2 value, 0.889 and the adjusted R^2 value, 0.977 is < 0.2 indicating that the results are in reasonable agreement with each other [41]. In addition, F -value of 2.03 indicates insignificant lack of fit.

Positive sign of regression coefficient indicates a synergistic effect while a negative value indicates antagonistic effect. In this study, the negative sign of coefficient of FeIII-NP dosage and positive sign of initial arsenic concentration indicates that response adsorption capacity increases as the dosage decreases and initial arsenic concentration increases under maximum adsorption capacity which is justified from Eq. (4).

On the other hand, pH is found to have no effect on the As(V) adsorption capacity. This can be well explained from the zeta potential data (Fig. 5) and the dissociation of As(V) [42]. Fig. 5 indicates presence of positive charge on the surface of the nanoparticles at lower pH values. The charge remains almost constant with the zeta potential value of about 43 mV for the experimental pH range of 6–8. Moreover, the redox potential versus pH diagram indicates that the charge of the ionated form of As(V) in the pH range remains almost same [43]. Since As(V) adsorption is basically a chemisorption process which occurs mainly due to the electrostatic interactions between positively charged adsorbent and negatively charged arsenate ions, adsorption capacity remains almost the same in the pH range of 6–8. The different complexes that may be formed on speciation of iron oxide with As(V) includes bidentate mononuclear, bidentate binuclear, and monodentate complex among which bidentate binuclear complexes have been reported to be thermodynamically stable [44];



$$(\text{p}K_a = 2.1) (\text{p}K_a = 6.7) (\text{p}K_a = 11.2)$$

The contour plots generated from RSM have been shown in Fig. 6(a–c) which reflects similar trends. It may be observed from these plots that the adsorption capacity increases with decrease in the FeIII-NP dosage and increases with increase in the initial arsenic concentration, however, pH is found to have no significant effect on the adsorption capacity.

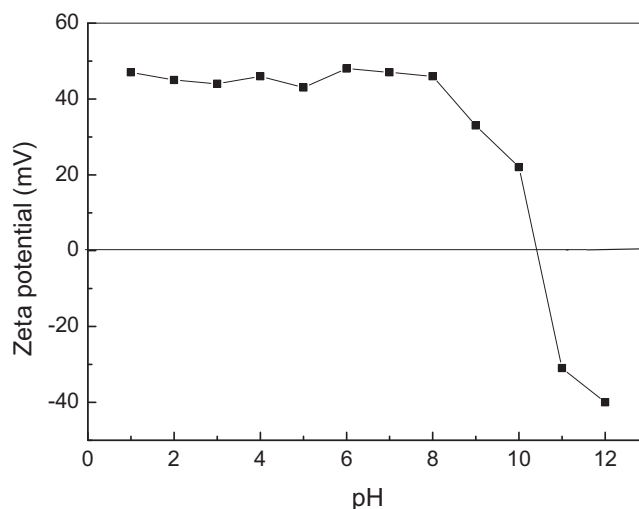


Fig. 5. Effect of pH on the surface charge of FeIII-NP.

Table 3
Analysis of variance for response of the adsorption capacity for As(V).

Source	Sum of squares	DF	Mean square	F Value	Prob > F
Model	60.55	9	6.73	81.55	<0.0001
A	4.531E-003	1	4.531E-003	0.055	0.8206
B	17.03	1	17.03	206.45	<0.0001
C	40.67	1	40.67	492.99	<0.0001
A ²	4.586E-003	1	4.586E-003	0.056	0.8195
B ²	1.57	1	1.57	19.07	0.0024
C ²	0.93	1	0.93	11.33	0.0098
AB	0.020	1	0.020	0.24	0.6343
AC	8.993E-004	1	8.993E-004	0.011	0.9194
BC	3.73	1	3.73	45.27	0.0001
Residual	0.66	8	0.082		
Lack of fit	0.51	5	0.10	2.03	0.2975
Pure error	0.15	3	0.050		
Cor total	68.02	19			

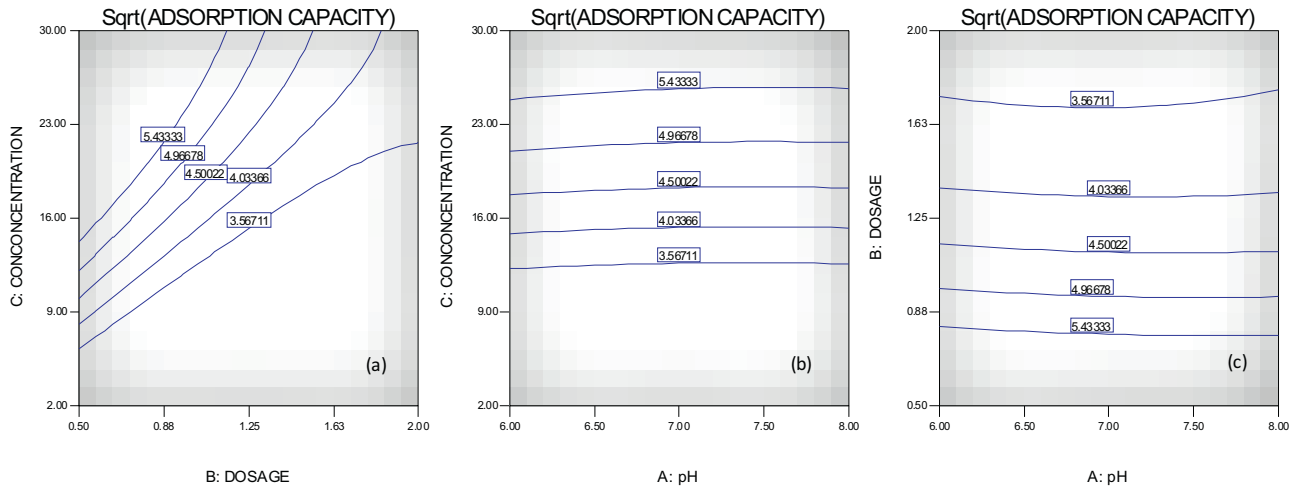


Fig. 6. Contour plots showing the effect of FeIII-NP dosage, initial arsenic(V) concentration and pH on arsenic(V) adsorption capacity.

Table 4

Optimized conditions as obtained from RSM.

Number	pH	Adsorbent dosage (g/L)	Initial As(V) concentration (mg/L)	Sqrt adsorption capacity (mg/g)	Desirability
Minimizing As(V) initial concentration					
1	6	0.50	2	2.534	1
2	6	0.52	2	2.487	0.997
3	6	0.50	2	2.532	0.97
4	6	0.64	2.15	2.187	0.963
5	6	0.50	5.13	3.570	0.952
Maximizing As(V) initial concentration					
6	6	0.5	30	8.084	1
7	6	0.51	30	8.048	0.998
8	6	0.52	29.98	8.0	0.996
9	6.02	0.51	29.62	8.001	0.994
10	6	0.51	29.42	7.957	0.99

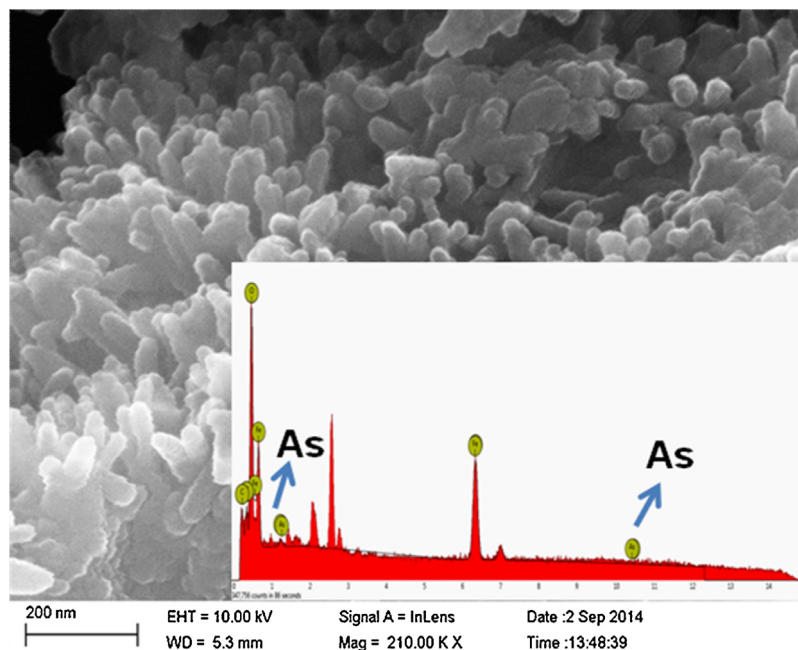


Fig. 7. FESEM image of FeIII-NP sample after As(V) adsorption with EDX analysis (inset).

3.4. Optimization of the parameters

Optimization of the parameters was done with the goal of both maximizing and minimizing the As(V) concentration keeping the pH and FeIII-NP dosage to a minimum level. The reason for such optimization is to obtain the best conditions for carrying out the adsorption process in different regions where the As(V) concentration may vary widely. The optimized conditions have been shown in Table 4. The desirability of the reported values is >0.95 which is acceptable.

3.5. Characterization of FeIII-NP after arsenic adsorption

FT-IR spectra of FeIII-NP sample (Fig. 4) indicates shifting of the peaks to 492 cm^{-1} and 692 cm^{-1} due to As(V) uptake by iron oxide nanoparticle [45,46]. A new band at 1375 cm^{-1} was observed which may be due to adsorption of As(V) on the nanoparticle [47]. The FESEM image in Fig. 7 shows agglomerated, cylindrical particles with partially reduced porosity. The EDX spectra showed As(V) peak reflecting arsenic uptake by the nanoparticle.

3.5.1. Adsorption isotherms

The adsorption process was carried out at 20, 30 and 40°C with varying initial arsenic concentrations from 5 mg/L to 30 mg/L. The adsorption data was fitted to Langmuir and Freundlich adsorption isotherm model as shown in Table 5. The value of R^2 was 0.98 in the linear fit indicating that the data fits well in Langmuir adsorption isotherm model compared to the Freundlich isotherm model suggesting monolayer adsorption. Moreover, the separation factor r , defined by $1/(1 + [K_L \times C_0])$ was always <1 indicating favourable adsorption.

3.5.2. Thermodynamic study

Gibbs free energy change ΔG^0 (J mol^{-1}), enthalpy change ΔH^0 (J mol^{-1}) and entropy change ΔS^0 ($\text{J mole}^{-1}\text{K}^{-1}$) are related by the following thermodynamic equations:

$$\Delta G^0 = \Delta H^0 - T\Delta S^0 \quad (7)$$

$$\text{Also, } \Delta G^0 = -RT \ln K_c \quad (8)$$

where R is the universal gas constant ($R = 8.314\text{ J mol}^{-1}\text{K}^{-1}$), T is the reaction temperature (K) and K_c is the equilibrium constant obtained from Langmuir adsorption isotherm. The values of ΔG^0 are obtained as -2326.657 , -2158.812 and $-2094.026\text{ J mole}^{-1}$ at 293 K, 303 K and 313 K, respectively. These negative values indicate the feasibility and spontaneous nature of the process. As evident from Eq. (8), the values of ΔH^0 and ΔS^0 can be obtained from the intercept and slope of the plot of ΔG^0 versus T . The value of ΔH^0 ,

$-22549.352\text{ J mol}^{-1}$ indicates the process to be exothermic in nature. The positive value of ΔS^0 , $69.147\text{ J mol}^{-1}\text{K}^{-1}$ indicates dissociative process and randomness at solid/solution interface during adsorption.

3.6. Kinetic study

The effect of contact time on adsorption of arsenic(V) by the synthesized iron oxide nanoparticles was investigated upto 240 min of adsorption with varying As(V) concentration of 5–20 mg/L. The experimental data indicates that the adsorption was rapid and almost completed within 45 min. The results obtained were fitted to Pseudo-first-order and Pseudo-second-order kinetic model. The values of all the parameters obtained have been represented in Table 6. The value of R^2 was 0.99 for the Pseudo-second-order model indicating a good linear fit compared to the Pseudo-first-order model. Thus, the uptake of As(V) ions on the iron oxide nanoparticle is basically the chemisorptive nature of adsorption on the active sites of the FeIII-NP surface.

3.7. Comparison of arsenic removal efficiency of Fe-NP with other inorganic oxide based adsorbents

Table 7 represents comparison of the efficiency of FeIII-NP for arsenic removal with other inorganic oxide based adsorbents under similar concentration range of As(V) [48–52]. It may be observed that green synthesized iron oxide nanoparticles shows considerable efficiency in comparison with the commercially available $\alpha\text{-Fe}_2\text{O}_3$ as well as with different forms of iron oxide nanostructures synthesized by chemical route. To further evaluate the efficiency of the nanoparticles for As (III) adsorption, experiments were carried out in the concentration range of 2 mg/L to 30 mg/L of As(III) solution with nanoparticle dosage of 1 g/L at pH of 6.5. From the results of Langmuir adsorption isotherm model fitting, the maximum adsorption capacity was found to be 41.98 mg/g which is reasonably high value [49]. Hence it may be concluded that phytochemicals rich extract of *A. vera* and a non-toxic precursor like FeCl_3 may be used for green synthesis of $\alpha\text{-Fe}_2\text{O}_3$ nanoparticle with high efficiency for arsenic removal.

3.8. Utilization of arsenic rich sludge in colored glass preparation

Glass has been considered as a safe and viable option for immobilization of toxic wastes like radioactive components from nuclear wastes. The main concept behind immobilization of toxic components in glass host is to provide a solid, stable, durable material that can either be safely disposed or reused for some beneficial purpose [53]. This is because glass has high chemical, heat, thermal and radiation resistance and do not degrade easily with change in environmental conditions. Hence, possibility of leaching of the constituents when exposed to harsh environmental

Table 5

Parameters obtained from Langmuir adsorption isotherm model and Freundlich adsorption isotherm model for As(V) adsorption.

Langmuir adsorption isotherm			
Temperature ($^\circ\text{C}$)	K_L (L/g)	q_m (mg/g)	R^2
20	2.599	38.475	0.985
30	2.356	36.263	0.983
40	2.236	35.461	0.9947
Freundlich adsorption isotherm			
Temperature ($^\circ\text{C}$)	K_f (mg/g)/(mg/L) $^{(1/n)}$	n	R^2
20	33.563	1.70	0.938
30	25.67	1.095	0.925
40	26.981	2.05	0.948

Table 6

Parameters obtained from Pseudo-first-order model and Pseudo-second-order model for As(V) adsorption.

Pseudo-second-order-model			
Initial As(V) concentration (mg/L)	K_f (mg/g)/(mg/L) $^{(1/n)}$	q_m (mg/g)	R^2
5	3.354	95.238	0.985
20	1.774	94.07	0.983
Pseudo-first-order-model			
Initial As(V) concentration (mg/L)	q_e (mg/g)	K (min^{-1})	R^2
5	0.259	0.0953	0.885
20	2.556	0.087	0.853

Table 7
Comparative study of As(V) adsorption capacity of different inorganic oxide adsorbents.

Adsorbent	Adsorption capacity (mg/g)	Initial As(V) concentrations (mg/L)
α -Fe ₂ O ₃	5.31	10
γ -Fe ₂ O ₃	4.75	
Fe ₃ O ₄	4.65	
Self-assembled 3D flower like iron oxide nanostructure [37]		
Activated alumina [38]	20.6	1–25
Sulphate modified iron oxide coated sand [39]	0.12	0.5–3.5
Commercial α -Fe ₂ O ₃ [36]	0.46	10
Starch stabilized nanoscale zerovalent iron [40]	12.2	0.25–10
Magnetite nanoparticles [46]	3.70	2
Green synthesized α-Fe₂O₃ (this study)	8.722	10
	38.475	2–30 (obtained from equilibrium isotherm study)

conditions is low. This prompted us to immobilize the arsenic containing iron oxide sludge in glass hosts and use it for beneficial purpose. Fe₂O₃ acts as a coloring agent in the process of glass formation. Fe is a transition metal having loosely bound 3d-electrons. The coloration in glass is due to strong absorptions of selective portions of visible wavelength regions of incident/transmitting electromagnetic radiation resulting from the occurrence of transitions between characteristic electronic energy level structures formed with the influence of ligand field. When Fe⁺³ cations are surrounded by anions O⁻², the interaction between the electric fields causes splitting of the energy levels. The number of the different levels formed is a function of the electronic configuration of the cation. The absorption of photons, having the same energy of split energy levels by electronic transitions between the split 3d levels results in visible coloration of the glass [54].

Iron in glass exists as equilibrium between the yellow ferrous Fe⁺² and bluish green ferric Fe⁺³ ions according to the following reaction:



The equilibrium of the reaction shifts to the right at higher temperature leading to ferrous ion formation. Fe⁺² and Fe⁺³ impart different color to the glass due to its different electronic configurations, Fe⁺² ([Ar] 3d⁶) Fe⁺³ ([Ar] 3d⁵). Due to the change in number of 3d electrons, different possible electronic transitions

lead to different absorption spectrums for Fe⁺²/Fe⁺³ ions. Hence, controlling factors like melting temperatures can lead to control of ratio of Fe⁺²/Fe⁺³ giving desired color to glass.

Attempt was made in present study to prepare colored soda lime silicate glass which may be used as container glass. Presence of ferrous/ferric ions formed during melting, imparts a green to bluish green or yellowish green color to the glass blocks prepared depending upon their redox ratio. The same arsenic containing iron oxide sludge may also be used to produce amber colored glasses which can be used as container glass for storage of various reagents, wine, etc. For this, carbon and sulphur need to be added along with the previously mentioned batch composition. Brown coloration is due to tetrahedral coordination of Fe⁺³ with three O⁻² and one S⁻². Carbon is added as a reducing agent to ensure the presence of S⁻² ions. The optical absorption is due to charge transfer process.

The prepared glasses appeared to be greenish blue. Both the glass blocks were examined for the bubbliness under microscope and the microscope images are depicted in Fig. 8. Normally bubbles may be formed in glass melting due to trapping of atmospheric gases or decomposition of the components during melting. Bubbles are considered as flaws in the glass making. The Fig. 8 clearly shows that the number, as well as, the size of bubbles is much reduced for the experimental block compared to the control. This is due to presence of arsenic in experimental block which acts as refining agent causing refining of the glass melt.

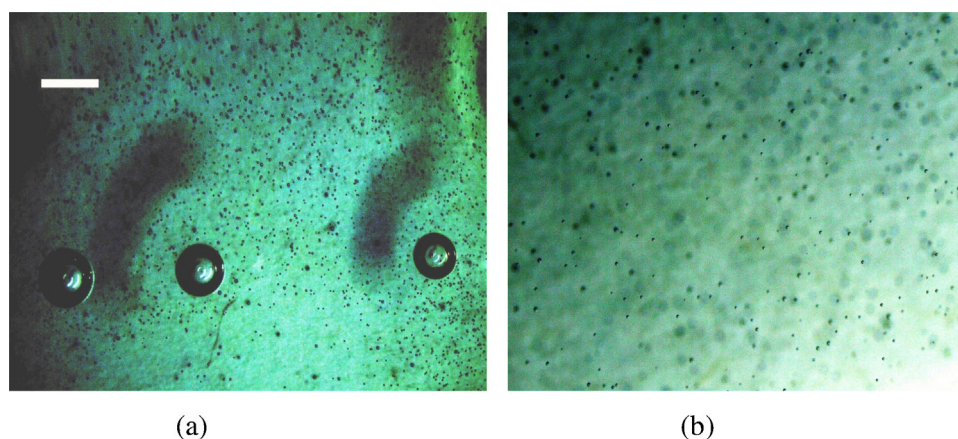


Fig. 8. Microscopic images of the prepared glass blocks (a) control (b) experimental. (For interpretation of the references to color in the text, the reader is referred to the web version of this article.)

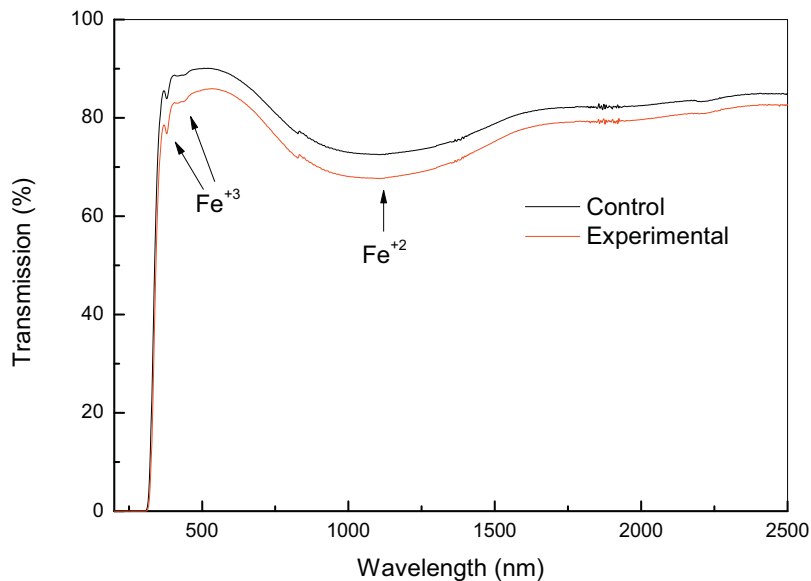
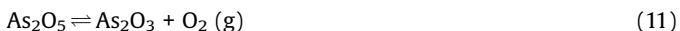


Fig. 9. Transmittance spectra of the prepared glass blocks.

Arsenic oxides act as a refining agent by causing reduction in bubbles [20]. At high temperature, the As_2O_5 decomposes according to the equations



The first reaction represented in Eq. (10) occurs during decomposition of starting raw materials in glass batch. This reaction forms large amounts of bubbles, which merge with each other, thus increasing their sizes which enhance their rate of rise to the surface. Later, during melting event at high temperature the formed As_2O_5 converts to As_2O_3 by releasing oxygen to the melt shown in Eq. (11). This released gas prompts the remaining small bubbles to grow bigger to rise to the melt surface for escape. Eq. (11) is a temperature dependent reaction. On lowering temperature, pentoxide species becomes stable for which it absorbs oxygen from the melt resulting in diffusion of oxygen

from left out bubbles, if any, thus causing shrinkage and extinction of the bubbles. This leads to refining of the glass melts which is well depicted in the figure.

The transmission spectra of glasses in Fig. 9 shows sharp absorption peak at 380 nm while two broad peaks at 420 nm and 436 nm were observed which may be attributed to the absorption peaks of ferric ion. Again, the presence of broad absorption peak at 1050 nm is due to the presence of ferrous ions [55]. Hence, the transmission spectra clearly shows the presence of ferric and ferrous ions as evident from Eq. (9). The intensity of the absorption peaks is higher compared to the normal soda lime silicate glasses. These indicate some absorption in the UV and the IR range for the iron oxide doped glasses, making it heat resistant and suitable for use as container glass. The density of the glasses as measured by Archimedes principle was estimated to be 2.49 g/cc for both the experimental and control samples.

The thermogravimetric plot in Fig. 10 shows no appreciable mass change on heating the sample till 950 °C. The differential thermal analysis of the experimental glass block showed peak at

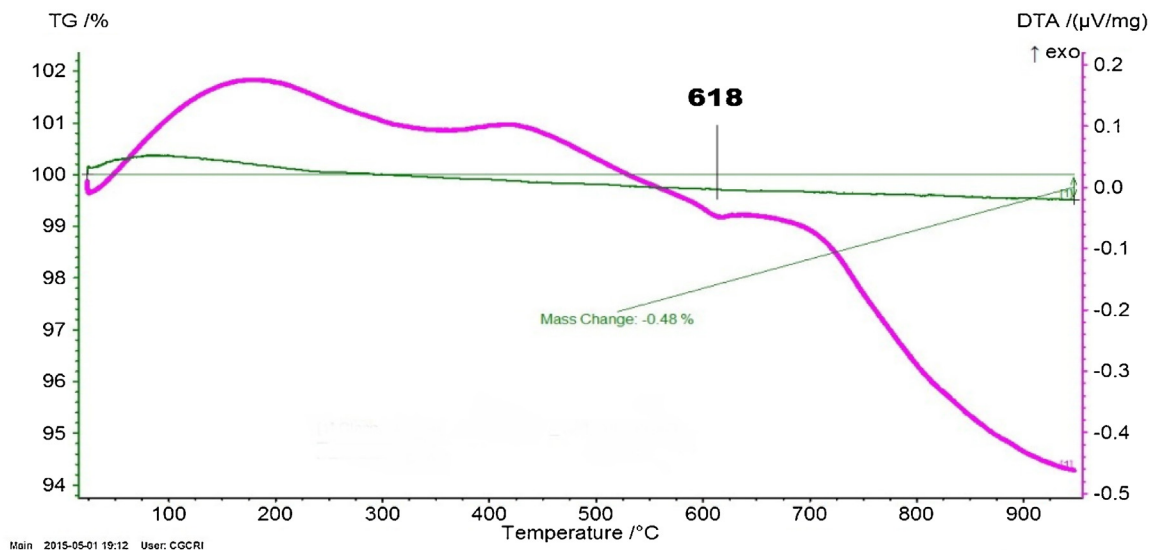


Fig. 10. TGA/DTA plot of the experimental glass block sample.

618 °C which is the indication of the glass transition temperature. The experimental soda lime silicate glass is suitable to be used in containers or any other suitable application, which is evident from all these important measured properties.

4. Conclusions

The comprehensive study reveals that plant extract of *A. vera* can be used for synthesis of iron oxide nanoparticles in a cost-effective, simple and eco-friendly route. X-ray diffraction proved that the particles are α -Fe₂O₃ having hexagonal phase, while the FESEM and TEM images indicated rod shaped particles with dimensions of about 100 nm. The as-synthesized nanoparticles showed high adsorption capacity for arsenic(V) compared to other reported inorganic adsorbents. The monolayer adsorption capacity at 20 °C was found to be 38.475 mg/g in the initial concentration range of 2–30 mg/L.

Response surface methodology based optimization study shows that initial arsenic concentration and particle dosage has major influence on the sorption capacity. However, pH does not have any significant effect within the experimental range. The ANNOVA analysis indicates that developed model as highly significant wherein, the experimental and predicted responses are in well agreement with *R*² value of 0.9828.

As(V) containing α -Fe₂O₃ nanoparticle sludge is utilized in the preparation of coloured soda lime silicate glass. Microscopic image of the glass block indicates that application of As sorbed nanoparticle sample reduces the number, as well as, the size of bubbles compared to that prepared from commercial Fe₂O₃ sample. Transmission spectra of glasses reveal absorption peaks with higher intensity compared to the normal soda lime silicate glasses and differential thermal analysis indicates high thermal stability.

It may be concluded that phytochemicals rich extract of *A. vera* and a non-toxic precursor like FeCl₃ may be used to synthesize Fe₂O₃ nanoparticles having high arsenic sorption capacity in comparison to the commercially available α -Fe₂O₃ and other forms of iron oxide nanostructures synthesized by chemical route. Application of these nanoparticles would be highly significant for arsenic removal application in drinking water. The spent nanoparticles may be safely utilized in colored glass preparation having applications like container bottles, building and ornamental glasses, etc. The entire study proposes a clean and green solution towards environmental remediation of toxic contaminant like arsenic.

Acknowledgement

The financial support from the Council of Scientific and Industrial Research (CSIR), Government of India, is gratefully acknowledged for completion of this work.

References

- [1] I. Ali, New generation adsorbents for water treatment, *Chem. Rev.* 112 (2012) 5073–5091.
- [2] W.X. Zhang, Nanoscale iron particles for environmental remediation: an overview, *J. Nanopart. Res.* 5 (2003) 323–332.
- [3] D. Zhang, S. Wei, C. Kaila, X. Su, J. Wu, A.B. Karki, D.P. Young, Z. Guo, Carbon-stabilized iron nanoparticles for environmental remediation, *Nanoscale* 2 (2010) 917–919.
- [4] J. Kong, K. Coolahan, A. Mugweru, Manganese based magnetic nanoparticles for heavy metal detection and environmental remediation, *Anal. Methods* 5 (2013) 5128–5133.
- [5] A. Goswami, P.K. Raul, M.K. Purkait, Arsenic adsorption using copper (II) oxide nanoparticles, *Chem. Eng. Res. Des.* 90 (2012) 1387–1396.
- [6] S. Aredes, B. Klein, M. Pawlik, The removal of arsenic from water using natural iron oxide minerals, *J. Clean. Prod.* 29–30 (2012) 208–213.
- [7] S. Sai Bhargav, I. Prabha, Removal of arsenic and copper metals from contaminated water using iron (III) oxide nanoparticle, *Int. J. Chem. Chem. Eng.* 2 (2013) 107–112.
- [8] P. Singh, S.K. Singh, J. Bajpai, A.K. Bajpai, R.B. Shrivastava, Iron crosslinked alginate as novel nanosorbents for removal of arsenic ions and bacteriological contamination from water, *J. Mater. Res. Technol.* 3 (2014) 195–202.
- [9] U. Beker, L. Cumbal, D. Duranoglu, I. Kucuk, A.K. Sengupta, Preparation of Fe oxide nanoparticles for environmental applications: arsenic removal, *Environ. Geochem. Health* 32 (2010) 291–296.
- [10] J. Yang, H. Zhang, M. Yu, I. Emmanuelawati, I. Zou, Z. Yuan, C. Yu, High-content, well-dispersed γ -Fe₂O₃ nanoparticles encapsulated in macroporous silica with superior arsenic removal performance, *Adv. Funct. Mater.* 24 (2014) 1354–1363.
- [11] R.K. Gupta, K. Ghosh, L. Dong, P.K. Kahol, Green synthesis of hematite (α -Fe₂O₃) submicron particles, *Mater. Lett.* 64 (2010) 2132–2134.
- [12] S. Irvani, Green synthesis of metal nanoparticles using plant, *Green Chem.* 13 (2011) 2638–2650.
- [13] M.S. Akhtar, J. Panwar, Y.Y. Sang, Biogenic synthesis of metallic nanoparticles by plant extracts, *ACS. Sustain. Chem. Eng.* 1 (2013) 591–602.
- [14] P. Yuvasree, K. Nithya, N. Neelakandeswari, Biosynthesis of Silver Nanoparticles from *Aloe Vera* Plant Extract and Its Antimicrobial Activity Against Multidrug Resistant Pathogens, Proceedings of the International Conference on Advanced Nanomaterials & Emerging Engineering Technologies, 2013.
- [15] C. Ragupathi, L.J. Kennedy, J.J. Vijaya, A new approach: synthesis, characterization and optical studies of nano-zinc aluminate, *Adv. Powder Technol.* 25 (2014) 267–273.
- [16] R. Herrera-Becerra, C. Zorrilla, J. Ascencio, Production of iron oxide nanoparticles by a biosynthesis method: an environmentally friendly route, *J. Phys. Chem. C* 111 (2007) 16147–16153.
- [17] X.G. Wen, S.H. Wang, Y. Ding, Z.L. Wang, S.H. Yang, Controlled growth of large-area uniform, vertically aligned arrays of α -Fe₂O₃ nanobelts and nanowires, *J. Phys. Chem. B* 109 (2005) 215–220.
- [18] L. Liu, H.Z. Kou, W.L. Mo, H.J. Liu, Y.Q. Wang, Surfactant-assisted synthesis of α -Fe₂O₃ nanotubes and nanorods with shape-dependent magnetic properties, *J. Phys. Chem. B* 110 (2006) 15218–15223.
- [19] J. Gu, S. Li, E. Wang, Q. Li, G. Sun, R. Xu, H. Zhang, Single-crystalline α -Fe₂O₃ with hierarchical structures: controllable synthesis, formation mechanism and photocatalytic properties, *J. Solid State Chem.* 182 (2009) 1265–1272.
- [20] S. Arunkumar, M. Muthuselvam, Analysis of phytochemical constituents and antimicrobial activities of *Aloe vera* L. against clinical pathogens, *World J. Agric. Sci.* 5 (2009) 572–576.
- [21] S.P. Chandran, M. Chaudhary, R. Pasricha, A. Ahmad, M. Sastry, Synthesis of gold nanotriangles and silver nanoparticles using *Aloe vera* plant extract, *Biotechnol. Prog.* 22 (2006) 577–583.
- [22] S. Medda, A. Hajra, U. Dey, P. Bose, N.K. Mondal, Biosynthesis of silver nanoparticles from *Aloe vera* leaf extract and antifungal activity against *Rhizopus* sp. and *Aspergillus* sp., *Appl. Nanosci.* (2014), doi:http://dx.doi.org/10.1007/s13204-014-0387-1.
- [23] H.M.A. Mahzuz, R. Alam, M.N. Alam, R. Basak, M.S. Islam, Use of arsenic contaminated sludge in making ornamental bricks, *Int. J. Environ. Sci. Tech.* 6 (2009) 291–298.
- [24] C. Stalhandske, Refining of lead glass using As(III)/Sb(III) or As(V)/Sb(V), *GLASTEKNISK TIDSKRIFT* 1999, nr 3, vol 54.
- [25] A. Criscuolo, S. Majumdar, A. Figoli, G.C. Sahoo, P. Bafaro, S. Bandyopadhyay, E. Drioloi, As (III) oxidation by MnO₂ coated PEEK-WC nanostructured capsules, *J. Hazard. Mat.* 211–212 (2012) 281–287.
- [26] G.E.P. Box, K.B. Wilson, On the experimental attainment of optimum conditions, *J. R. Stat. Soc. B* 13 (1951) 1–45.
- [27] S.L.C. Ferreira, R.E. Bruns, E.G.P. da Silva, W.N.L. dos Santos, C.M. Quintella, J.M. David, J.B. de Andrade, M.C. Breitenkreitz, I.C.S.F. Jardim, B.B. Neto, Statistical designs and response surface techniques for the optimization of chromatographic systems, *J. Chromatogr. A* 1158 (2007) 2–14.
- [28] M.A. Bezerra, R.E. Santelli, E.P. Oliveira, L.S. Villar, L.A. Escalera, Response surface methodology (RSM) as a tool for optimization in analytical chemistry, *Talanta* 76 (2008) 965–977.
- [29] D. Ranjan, D. Mishra, S.H. Hasan, Bioadsorption of arsenic: an artificial neural networks and response surface methodological approach, *Ind. Eng. Chem. Res.* 50 (2011) 9852–9863.
- [30] S.K. Ponnusamy, R. Subramaniam, Process optimization studies of Congo red dye adsorption onto cashew nut shell using response surface methodology, *Int. J. Ind. Chem.* 4 (2013) 17.
- [31] P.R. Sajanlal, T.S. Sreerasad, A.K. Samal, T. Pradeep, Anisotropic nanomaterials: structure, growth, assembly, and functions, *Nano Rev.* 2 (2011), doi:http://dx.doi.org/10.3402/nano.v2i0.5883.
- [32] A.P. Grosvenor, B.A. Kobe, M.C. Biesinger, N.S. McIntyre, Investigation of multiplet splitting of Fe 2p XPS spectra and bonding in iron compounds, *Surf. Interface. Anal.* 36 (2004) 1564–1574.
- [33] J.F. Moulder, W.F. Stickle, P.E., Sobol, K.D. Bomben, Handbook of X-ray photoelectron spectroscopy (1995) Minnesota, USA.
- [34] G. Beamson, D. Briggs, High Resolution XPS of Organic Polymers—The Scienta ESCA300 Database, Wiley Interscience, 1992 Appendices 3.1 and 3.2.
- [35] M.M. Rahman, S.B. Khan, A. Jamal, M. Faisal, A.M. Aisiri, Iron oxide nanoparticles, *J. Nano Mat.*, (2011), Prof. Mohammed Rahman (Ed.), ISBN: 978-953-307-913-4, InTech.

- [36] D. Zhao, G. Liu, D. Song, J.H. Liu, Y. Zhou, J. Ou, S. Shizhong, Fourier transform infrared spectroscopic study of truffles, *ICO20: Biomedical Optics*, edited by Gert von Bally, Qingming Luo, Proc. of SPIE Vol. 6026, 60260H 0277-786X/06/\$15 (2006) doi: 10.1117/12.667133.
- [37] P. Sutradhar, N. Debnath, M. Saha, Microwave-assisted rapid synthesis of alumina nanoparticles using tea, coffee and triphala extracts, *Adv. Manuf.* 1 (2013) 357–361.
- [38] J.H. Hamman, Composition and applications of *Aloe vera* leaf gel, *Molecules* 13 (2008) 1599–1616.
- [39] M. Ahmed, F. Hussain, Chemical composition and biochemical activity of *Aloe vera* (*Aloe barbadensis* Miller) leaves, *Int. J. Chem. Biochem. Sci.* 3 (2013) 29–33.
- [40] A. Alves, C.P. Bergmann, F.A. Berutti, Combustion synthesis, novel synthesis and characterization of nanostructured materials, *Engineering Materials*, Springer-Verlag, Berlin Heidelberg, 2013, doi:http://dx.doi.org/10.1007/978-3-642-41275-2_2 Chapter 2.
- [41] M. Mourabet, A. Rhilassi, H. Boujaady, M. Bennani-Ziatni, A. Taitaiet, Use of response surface methodology for optimization of fluoride adsorption in an aqueous solution by Brushite, *Arabian J. Chem.* (2014), doi:http://dx.doi.org/10.1016/j.arabjc.2013.12.028.
- [42] D. Mohan, C.U. Pittman, Arsenic removal from water/wastewater using adsorbents—a critical review, *J. Hazard. Mat.* 142 (2007) 1–53.
- [43] D.M. Martin, Supermagnetic iron oxide nanoparticles as arsenic adsorbent, Doctoral thesis, University Autònoma de Barcelona, (2013).
- [44] I. Carabante, Arsenic(V) Adsorption on iron oxide implications for soil remediation and water purification, Doctoral Thesis, Lulea University of Technology, Sweden, 2012, pp. 11–26.
- [45] S. Goldberg, C.T. Johnston, Mechanisms of arsenic adsorption on amorphous oxides evaluated using macroscopic measurements, vibrational spectroscopy, and surface complexation modeling, *J. Colloid Interface Sci.* 234 (2001) 204–216.
- [46] S.C.B. Myneni, S.J. Traina, G.A. Waychunas, T.J. Logan, Vibrational spectroscopy of functional group chemistry and arsenate coordination in ettringite, *Geochim. Cosmochim. Acta* 62 (1998) 3499–3514.
- [47] F.A. Miller, C.H. Wilkins, Infrared spectra and characteristic frequencies of inorganic ions, their use in qualitative analysis, *Anal. Chem.* (1952) 1253–1294.
- [48] L.S. Zhong, J.S. Hu, H.P. Liang, A.M. Cao, W.G. Song, L.J. Wan, Self-assembled 3D flowerlike iron oxide nanostructures and their application in water treatment, *Adv. Mater.* 18 (2006) 2426–2431.
- [49] S.S. Tripathy, A.M. Raichur, Enhanced adsorption capacity of activated alumina by impregnation with alum for removal of As(V) from water, *Chem. Eng. J.* 138 (2008) 179–186.
- [50] R.C. Vaishya, S.K. Gupta, Modeling arsenic (III) adsorption from water by sulfate modified iron-oxide coated sand (SMIOCS), *Sci. Technol.* 39 (2004) 645–666.
- [51] M. Mosfer, S. Nemati, A. Khataee, S. Nasser, A.A. Hashemi, Removal of Arsenic (III, V) from aqueous solution by nanoscale zero-valent iron stabilized with starch and carboxymethyl cellulose, *J. Env. Health. Sci. Eng.* 12 (2014) 74.
- [52] S.R. Chowdhury, E.K. Yanful, Arsenic removal from aqueous solutions by adsorption on magnetite nanoparticles, *Water Environ. J.* 25 (2011) 429–437.
- [53] W. Donald, B.L. Metcalfe, R.N.J. Taylor, The immobilization of high level radioactive wastes using ceramics and glasses, *J. Mater. Sci.* 32 (1997) 5851–5887.
- [54] J.E. Shelby, *Introduction to Glass Science and Technology*, Royal Society of Chemistry, Cambridge, 2005, pp. 208–211.
- [55] B. Mehdikhani, G.H. Borhani, Optical spectroscopy of sodium silicate glasses prepared with nano- and micro-sized iron oxide particles, *Process. Appl. Ceram.* 7 (2013) 117–121.